Article

Electrocatalytic Hydrogen Evolution at Low Overpotentials by Cobalt Macrocyclic Glyoxime and Tetraimine Complexes

Xile Hu, Bruce S. Brunschwig, and Jonas C. Peters

J. Am. Chem. Soc., **2007**, 129 (29), 8988-8998• DOI: 10.1021/ja067876b • Publication Date (Web): 28 June 2007

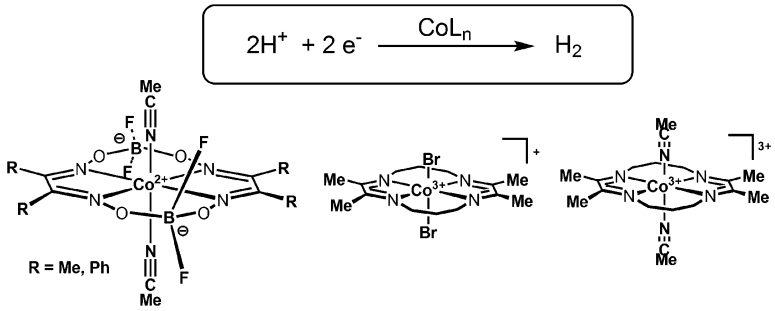

More About This Article

Additional resources and features associated with this article are available within the HTML version:

- Supporting Information
- Links to the 13 articles that cite this article, as of the time of this article download
- Access to high resolution figures
- Links to articles and content related to this article
- Copyright permission to reproduce figures and/or text from this article

View the Full Text HTML

J|A|C|S
ARTICLES
Published on Web 06/28/2007

Electrocatalytic Hydrogen Evolution at Low Overpotentials by Cobalt Macrocyclic Glyoxime and Tetraimine Complexes

Xile Hu, Bruce S. Brunschwig, and Jonas C. Peters*

Contribution from the Arnold and Mabel Beckman Laboratories of Chemical Synthesis and the Beckman Institute, Division of Chemistry and Chemical Engineering, California Institute of Technology, MC 127-72, Pasadena, California 91125

Received November 3, 2006; E-mail: jpeters@caltech.edu

Abstract: Cobalt complexes supported by diglyoxime ligands of the type $Co(dmgBF_2)_2(CH_3CN)_2$ and $Co(dpgBF_2)_2(CH_3CN)_2$ (where $dmgBF_2$ is difluoroboryl-dimethylglyoxime and $dpgBF_2$ is difluoroboryl-diphenylglyoxime), as well as cobalt complexes with [14]-tetraene-N_4 (Tim) ligands of the type $[Co(Tim^R)X_2]^{n+}$ (R = methyl or phenyl, X = Br or CH_3CN; $n = 1$ with X = Br and $n = 3$ with X = CH_3CN), have been observed to evolve H_2 electrocatalytically at potentials between −0.55 V and −0.20 V vs SCE in CH_3CN. The complexes with more positive Co(II/I) redox potentials exhibited lower activity for H_2 production. For the complexes $Co(dmgBF_2)_2(CH_3CN)_2$, $Co(dpgBF_2)_2(CH_3CN)_2$, $[Co(Tim^{Me})Br_2]Br$, and $[Co(Tim^{Me})(CH_3CN)_2](BPh_4)_3$, bulk electrolysis confirmed the catalytic nature of the process, with turnover numbers in excess of 5 and essentially quantitative faradaic yields for H_2 production. In contrast, the complexes $[Co(Tim^{Ph/Me})Br_2]Br$ and $[Co(Tim^{Ph/Me})(CH_3CN)_2](BPh_4)_3$ were less stable, and bulk electrolysis only produced faradaic yields for H_2 production of 20−25%. Cyclic voltammetry of $Co(dmgBF_2)_2(CH_3CN)_2$, $[Co(Tim^{Me})Br_2]^+$, and $[Co(Tim^{Me})(CH_3CN)_2]^{3+}$ in the presence of acid revealed redox waves consistent with the Co(III)−H/Co(II)−H couple, suggesting the presence of Co(III) hydride intermediates in the catalytic system. The potentials at which these Co complexes catalyzed H_2 evolution were close to the reported thermodynamic potentials for the production of H_2 from protons in CH_3CN, with the smallest overpotential being 40 mV for $Co(dmgBF_2)_2(CH_3CN)_2$ determined by electrochemistry. Consistent with this small overpotential, $Co(dmgBF_2)_2(CH_3CN)_2$ was also able to oxidize H_2 in the presence of a suitable conjugate base. Digital simulations of the electrochemical data were used to study the mechanism of H_2 evolution catalysis, and these studies are discussed.

1. Introduction

The development of robust hydrogen evolution catalysts that are made of inexpensive and earth abundant materials is of considerable current interest.[1] Fe−Ni and Fe−Fe hydrogenases produce dihydrogen in water at close to the thermodynamic potential of −0.41 V vs the normal hydrogen electrode (NHE) at pH = 7.[2] However, most known molecular H_2 evolution catalysts, based either on the structure of the active site of hydrogenases[3] or on metal complexes having simple macrocyclic ligands,[4−6] catalyze H_2 evolution in organic solvents at fairly negative potentials, from ∼ −1.1 to −2 V vs a saturated calomel electrode (SCE).[7]

A select number of molecular systems reported to date show promise for H_2 evolution at more positive potentials. DuBois et al. have shown that a $Cp_2Mo_2S_2$ system catalyzes electrochemical H_2 evolution at −0.26 V vs SCE in CH_3CN using *p*-cyanoanilinium as the acid source, and a $[Ni(P^{Ph}_2N^{Ph}_2)(CH_3$-

(1) Gratzel, M. *Acc. Chem. Res.* **1981**, *14*, 376−384. Bard, A. J.; Fox, M. A. *Acc. Chem. Res.* **1995**, *28*, 141−145. Khaselev, O.; Turner, J. A. *Science* **1998**, *280*, 425−427. Khan, S. U. M.; Al-Shahry, M.; Ingler, W. B. *Science* **2002**, *297*, 2243−2245. Zou, Z. G.; Ye, J. H.; Sayama, K.; Arakawa, H. *Nature* **2001**, *414*, 625−627. Maeda, K.; Teramura, K.; Lu, D. L.; Takata, T.; Saito, N.; Inoue, Y.; Domen, K. *Nature* **2006**, *440*, 295−295. Dempsey, J. L.; Esswein, A. J.; Manke, D. R.; Rosenthal, J.; Soper, J. D.; Nocera, D. G. *Inorg. Chem.* **2005**, *44*, 6879−6892. Lewis, N. S.; Nocera, D. G. *Proc. Natl. Acad. Sci. U.S.A.* **2006**, *103*, 15729−15735. US DOE Hydrogen Program: http://www.hydrogen.energy.gov/; "Basic Research Needs for the Hydrogen Economy"; available at http://www.sc.doe.gov/bes/reports/files/NHE_rpt.pdf; Powering the Planet: A Chemical Bonding Center. Website: http://www.caltechmitsolarpower.caltech.edu/.

(2) Adams, M. W. W. *Biochim. Biophys. Acta* **1990**, *1020*, 115−145. Frey, M. In *Structure and Bonding*; Hill, H. A. O., Sadler, P. J., Thomson, A. J., Eds; Springer-Verlag: Berlin, New York, 1997; Vol. 90, pp 97−126. Adams, M. W. W.; Stiefel, E. I. *Science* **1998**, *282*, 1842−1843. Fontecilla-Camps, J. C.; Ragsdale, S. W. In *Advances in Inorganic Chemistry*; Sykes, A. G., Ed.; Academic Press: 1999; Vol 47, pp 283−333. Peters, J. W.; Lanzilotta, W. N.; Lemon, B. J.; Seefeldt, L. C. *Science* **1998**, *282*, 1853−1858. Darensbourg, M. Y.; Lyon, E. J.; Smee, J. J. *Coord. Chem. Rev.* **2000**, *206*, 533−561.

(3) Tard, C.; Liu, X. M.; Ibrahim, S. K.; Bruschi, M.; De Gioia, L.; Davies, S. C.; Yang, X.; Wang, L. S.; Sawers, G.; Pickett, C. J. *Nature* **2005**, *433*, 610−613. Gloaguen, F.; Lawrence, J. D.; Rauchfuss, T. B. *J. Am. Chem. Soc.* **2001**, *123*, 9476−9477. Darensbourg, M. Y.; Lyon, E. J.; Zhao, X.; Georgakaki, I. P. *Proc. Natl. Acad. Sci. U.S.A.* **2003**, *100*, 3683−3688. Ott, S.; Kritikos, M.; Akermark, B.; Sun, L. C.; Lomoth, R. *Angew. Chem., Int. Ed.* **2004**, *43*, 1006−1009.

(4) Fisher, B.; Eisenberg, R. *J. Am. Chem. Soc.* **1980**, *102*, 7361−7363. Beley, M.; Collin, J. P.; Ruppert, R.; Sauvage, J. P. *J. Chem. Soc., Chem. Commun.* **1984**, 1315−1316. Collin, J. P.; Jouaiti, A.; Sauvage, J. P. *Inorg. Chem.* **1988**, *27*, 1986−1990. Efros, L. L.; Thorp, H. H.; Brudvig, G. W.; Crabtree, R. H. *Inorg. Chem.* **1992**, *31*, 1722−1724. Koelle, U. *New J. Chem.* **1992**, *16*, 157−169. Collman, J. P.; Wagenknecht, P. S.; Lewis, N. S. *J. Am. Chem. Soc.* **1992**, *114*, 5665−5673. Grass, V.; Lexa, D.; Saveant, J. M. *J. Am. Chem. Soc.* **1997**, *119*, 7526−7532.

(5) Collman, J. P.; Ha, Y. Y.; Wagenknecht, P. S.; Lopez, M. A.; Guilard, R. *J. Am. Chem. Soc.* **1993**, *115*, 9080−9088.

(6) Bhugun, I.; Lexa, D.; Saveant, J. M. *J. Am. Chem. Soc.* **1996**, *118*, 3982−3983.

(7) Unless otherwise noted, all potentials are referenced against SCE. NHE vs SCE = −0.24 V in aqueous solution; ferrocenium/ferrocene vs SCE = 0.38 V in acetonitrile.

10.1021/ja067876b CCC: $37.00

Scheme 1. Cobalt Difluoroboryl-Diglyoximate Complexes **1**−**3**

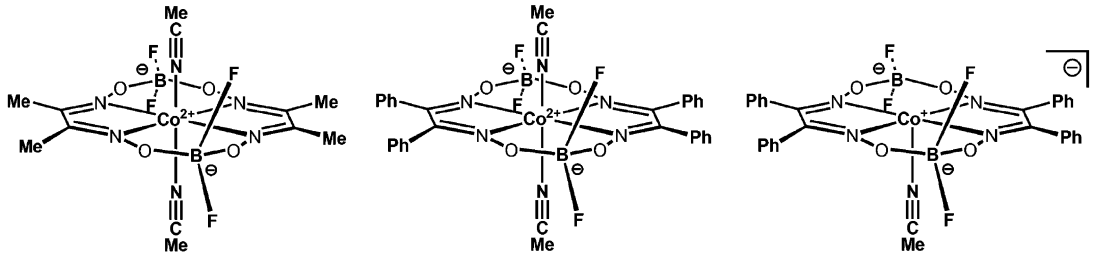

1 **2** **3**

CN)]$^{2+}$ system catalyzes H_2 evolution at −0.46 V vs SCE using triflic acid as the acid source.[8,9] We and others have shown that Co(diglyoxime) complexes evolve H_2 at relatively positive potentials either catalytically or electrocatalytically.[10−12] For example, Co(dmgBF$_2$)$_2$(CH$_3$CN)$_2$ (**1**, dmgBF$_2$ = difluoroboryl-dimethylglyoxime)[11] catalyzes H_2 evolution in acidic CH_3CN at −0.55 V vs SCE using CF_3COOH or HCl as the acid source, whereas Co(dpgBF$_2$)$_2$(CH$_3$CN)$_2$ (**2**, dpgBF$_2$ = difluoroboryl-diphenylglyoxime)[13] produces H_2 at even higher potentials (−0.28 V vs SCE) in acidic CH_3CN using HCl or HBF_4·Et_2O as the acid source (Scheme 1). Similarly, Artero et al. have shown that [Co(dmgH)$_2$PyCl](dmgH = dimethylglyoxime) catalyzes H_2 evolution at −1.03 V vs SCE in acidic DMF solutions using Et_3NHCl as the acid source.[12]

In this work, we report the electrochemical and electrocatalytic behavior of a series of cobalt complexes having BF_2-bridged diglyoxime or propane-bridged macrocyclic tetraimine ligands. The behavior of this series of complexes has allowed for the formulation of a correlation between the activity of H_2 evolution and the $Co^{II/I}$ reduction potentials of the various complexes. Electrochemical evidence for Co(III) hydride intermediates is presented, and a plausible mechanism of the H_2 evolution reaction is discussed. Furthermore, complex **1**, Co(dmgBF$_2$)$_2$(CH$_3$CN)$_2$, is shown to be a molecular catalyst able to mediate both H_2 evolution and oxidation, confirming its low overpotential for H_2 evolution. To the best of our knowledge, this is the first such demonstration to be reported for a synthetic catalyst.

2. Results

2.1. Electrocatalytic H_2 Evolution by Cobalt Difluoroboryl-Diglyoximate Complexes 1 and 2. Figure 1 shows the cyclic voltammogram (CV) of **1** (0.3 mM, 0.1 M [^{n}Bu$_4$N][ClO$_4$], CH_3CN) at a glassy carbon electrode. The reversible redox process shown at −0.55 V vs SCE in the absence of acid was assigned to the $Co^{II/I}$ couple. Upon addition of the monohydrate of toluenesulfonic acid (tosic acid, TsOH·H_2O), a catalytic wave was observed at a potential close to the formal reduction potential, $E^{\circ\prime}(Co^{II/I})$, for **1**. At low acid concentrations, the catalytic wave exhibited a peak-like shape, indicating that the catalytic reaction proceeded sufficiently rapidly that the concentration of acid was attenuated close to the electrode and that the current was controlled, at least partially, by diffusion of acid to the electrode surface.[14−16] At higher acid concentrations (e.g., 9 mM), the catalytic wave approached a plateau shape. The potential at which catalysis occurred did not change as the acid concentration was varied. The cyclic voltammetry of a 0.6 mM solution of **2** (glassy carbon electrode, 0.1 M [^{n}Bu$_4$N][ClO$_4$], CH_3CN) was similar to that of **1** (Figure 2), indicating that **2** is also an electrocatalyst for H_2 evolution.

In the absence of a catalyst, the direct reduction of acid at a glassy carbon electrode in solutions containing tosic acid took place at potentials more negative than −1.0 V vs SCE, and the background current was found to be negligible at the potentials where catalysis occurred using catalyst **1** or **2**. The rise in the catalytic current at −0.6 V vs SCE in Figure 2 is due to the tail of the catalytic wave originating from a Co(III)−H intermediate (vide infra).

2.2. Structural Characterization of Complexes 2 and 3. The solid-state molecular structure of the Co(II) form of catalyst **2** was determined by X-ray crystallography (Figure 3). The refined structure reveals a six-coordinate cobalt(II) ion that is ligated by a planar difluoroboryl-diglyoxime ligand and by two trans-oriented acetonitrile molecules. The cobalt ion is located on a crystallographically defined inversion center. The observed axial Co−$N_{nitrile}$ distance of 2.241(3) Å is much longer than the 1.886(5) Å averaged Co−N_{imine} distance in the glyoxime plane.

The Co(I) form of the complexes can be conveniently synthesized by chemical methods. For instance, [Co(dpgBF$_2$)$_2$(CH$_3$CN)]$^-$ (**3**) was synthesized by reducing **2** with 1 equiv of Na/Hg or Co(Cp)$_2$ in CH_3CN. The refined solid-state molecular structure of **3** (Figure 4) contains a five-coordinate cobalt(I) center in a distorted square-pyramidal ligand environment. The Co−$N_{nitrile}$ distance is 1.973(2) Å for **3**, 0.268 Å shorter than that in **2**. Because of this strong Co−$N_{nitrile}$ interaction, the cobalt ion is displaced 0.27 Å toward the nitrile ligand from the plane defined by the macrocyclic imine ligand. The average Co−N_{imine} distance of 1.851(6) Å for **3** is slightly shorter (0.035 Å) than that in **2**, consistent with expectations for a higher degree of metal to ligand π-backbonding.

2.3. Electrocatalytic H_2 Evolution by Cobalt Macrocyclic Tetraimine Complexes 4a−6b. Complexes **4a**−**6b**[17−20] (Scheme

(8) Appel, A. M.; DuBois, D. L.; DuBois, M. R. *J. Am. Chem. Soc.* **2005**, *127*, 12717−12726.
(9) Wilson, A. D.; Newell, R. H.; McNevin, M. J.; Muckerman, J. T.; DuBois, M. R.; DuBois, D. L. *J. Am. Chem. Soc.* **2006**, *128*, 358−366.
(10) Hu, X. L.; Cossairt, B. M.; Brunschwig, B. S.; Lewis, N. S.; Peters, J. C. *Chem. Commun.* **2005**, 4723−4725.
(11) Connolly, P.; Espenson, J. H. *Inorg. Chem.* **1986**, *25*, 2684−2688.
(12) Artero, V.; Fontecave, M. *Coord. Chem. Rev.* **2005**, *249*, 1518−1535; Razavet, M.; Artero, V.; Fontecave, M. *Inorg. Chem.* **2005**, *44*, 4786−4795.
(13) Tovrog, B. S.; Kitko, D. J.; Drago, R. S. *J. Am. Chem. Soc.* **1976**, *98*, 5144−5153.
(14) Bard, A. J.; Faulkner, L. R. *Electrochemical Methods: Fundamentals and Applications*, 2nd ed.; John Wiley & Sons, Inc.: New York, 2001.
(15) Andrieux, C. P.; Blocman, C.; Dumasbouchiat, J. M.; Mhalla, F.; Saveant, J. M. *J. Electroanal. Chem.* **1980**, *113*, 19−40.
(16) Saveant, J. M.; Su, K. B. *J. Electroanal. Chem.* **1984**, *171*, 341−349.
(17) Tait, A. M.; Busch, D. E. In *Inorganic Syntheses*; Douglas, B. E., Ed.; Wiley-Interscience: New York, 1978; Vol. XVIII, pp 22−26.

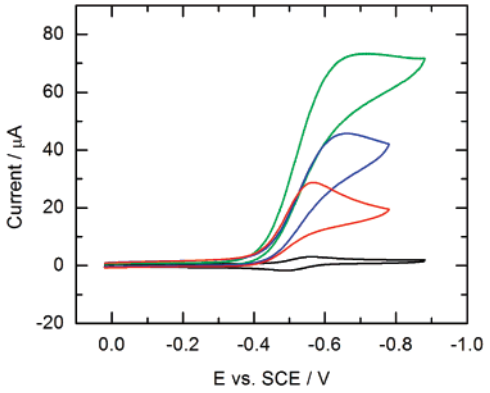

Figure 1. Cyclic voltammogram of complex **1** in CH_3CN solution containing 0.1 M [^{n}Bu$_4$N][ClO_4] in the presence of tosic acid: 0.3 mM **1** and no acid (black), 1.5 mM TsOH·H_2O (red), 4.5 mM TsOH·H_2O (blue), and 9 mM TsOH·H_2O (green). Scan rate: 100 mV/s; glassy carbon electrode.

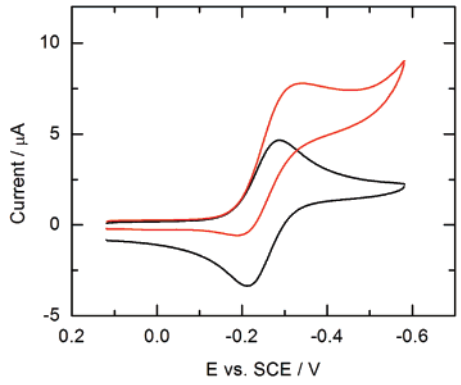

Figure 2. Cyclic voltammogram of 0.6 mM **2** in CH_3CN solution containing 0.1 M [^{n}Bu$_4$N][ClO_4] in the absence (black) and presence (red) of 9 mM TsOH·H_2O. Scan rate: 100 mV/s; glassy carbon electrode.

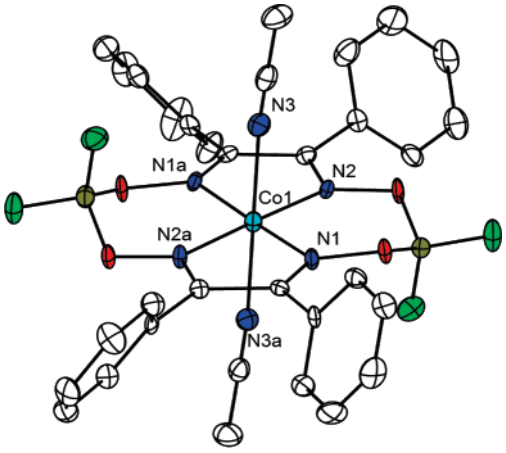

Figure 3. Solid-state molecular structure of the anion of **2**. Hydrogen atoms and two CH_2Cl_2 molecules of cocrystallization have been omitted for clarity; thermal ellipsoids are displayed at the 50% probability. Selected bond lengths (Å) and angles (deg): Co1−N1, 1.882(3); Co1−N2, 1.889(3); Co1−N3, 2.241(3); N1−Co1−N2, 98.33(19); N2−Co1−N1a, 81.78(12); N1−Co1−N3, 98.33(12); N2−Co1−N3, 81.63(12).

2) each exhibited reversible cyclic voltammetric behavior for the $Co^{II/I}$ redox couple, with $E^{o\prime}(Co^{II/I})$ values vs SCE in CH_3CN of −0.38 V for **4a**, −0.35 V for **4b**, −0.25 V for **5a**, −0.20 V for **5b**, −0.15 V for **6a**, and −0.08 V for **6b**. The value of $E^{o\prime}(Co^{II/I})$ shifted by ∼60 mV as a result of each substitution of a methyl group on the Tim ligand by the more electron-withdrawing phenyl group. This potential shift is comparable to the ∼65 mV potential shift that results from the substitution of phenyl for methyl in the cobalt difluoroboryl-diglyoxime complexes, **1** vs **2**. Substitution of two anionic bromide ligands by two neutral acetonitrile ligands shifted the potential by 20, 50, and 70 mV for **4a** to **4b**, **5a** to **5b**, and **6a** to **6b**, respectively. The axial bromide ligands in **4a**, **5a**, and **6a** were not replaced by acetonitrile upon dissolution in acetonitrile, as such solutions remained green, indicative of the bromide complexes, rather than turning pale-yellow indicative of the acetonitrile adduct complexes. All bromide complexes exhibited reversible $Co^{III/II}$

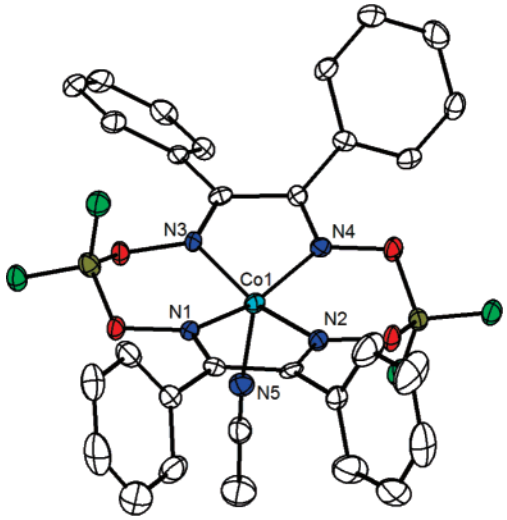

Figure 4. Solid-state structure of the anion of **3·Na(12-crown-4)$_2$**. Hydrogen atoms, the Na(12-crown-4)$_2^+$ countercation, and cocrystallization solvent molecules have been omitted for clarity; thermal ellipsoids are displayed at the 50% probability. Selected bond lengths (Å) and angles (deg): Co1−N1, 1.853(2); Co1−N2, 1.846(2); Co1−N3, 1.859(2); Co1−N4, 1.846(2); Co1−N5, 1.973(2); N1−Co1−N2, 80.83(8); N2−Co1−N4, 95.59(8); N3−Co1−N4, 81.13(8); N3−Co1−N1, 95.34(8); N1−Co1−N5, 96.54(8); N2−Co1−N5, 102.16(8); N3−Co1−N5, 103.44(8); N4−Co1−N5, 98.39(8).

Scheme 2. Cobalt Complexes of [14]-Tetraene-N_4 Ligands **4a**−**6b**

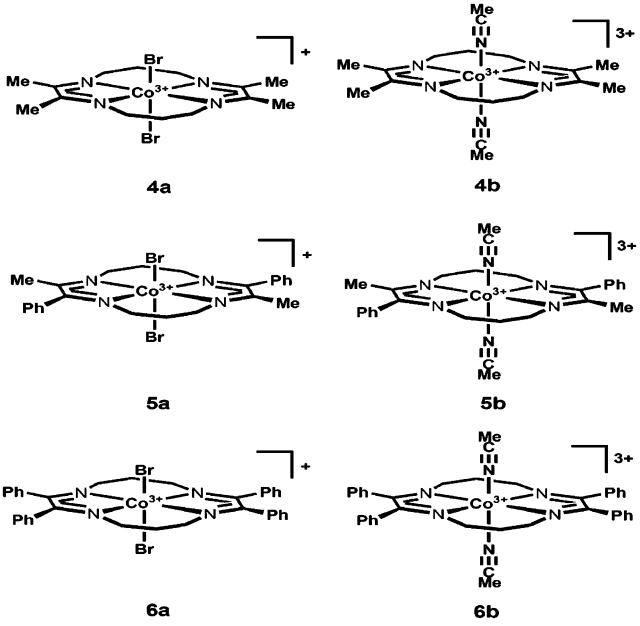

(18) Welsh, W. A.; Reynolds, G. J.; Henry, P. M. *Inorg. Chem.* **1977**, *16*, 2558−2561.
(19) Kildahl, N. K.; Antonopoulos, G. *J. Coord. Chem.* **1986**, *14*, 293−307.
(20) Eggleston, D. S.; Jackels, S. C. *Inorg. Chem.* **1980**, *19*, 1593−1599.

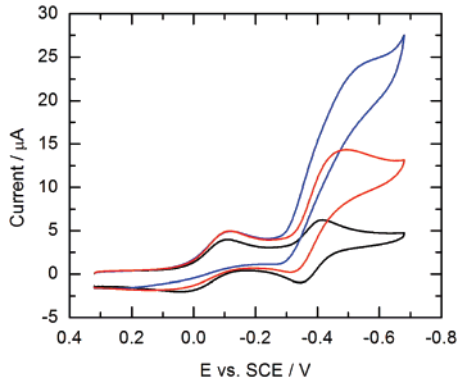

Figure 5. Cyclic voltammogram of complex **4a** in CH_3CN solutions containing 0.1 M [^{n}Bu$_4$N][ClO_4] in the presence of acid: 0.15 mM **1** and no acid (black), 1.5 mM TsOH·H_2O (red), and 9 mM TsOH·H_2O (blue). Scan rate: 100 mV/s; glassy carbon electrode.

couples (Table 2), while all acetonitrile complexes exhibited no redox waves for their $Co^{III/II}$ couples between 0.3 V to −1 V vs SCE. This suggests that the bromide ligands of complexes **4a**, **5a**, and **6a** are not substituted by acetonitrile even in their Co(II) form on the time scale of the CV measurements.

Figure 5 shows the CV of **4a**. In CH_3CN with 0.1 M [^{n}Bu$_4$N][ClO_4], reversible reductions were observed for the $Co^{III/II}$ couple at −0.06 V vs SCE and for the $Co^{II/I}$ couple at −0.38 V vs SCE. Addition of TsOH·H_2O to an unstirred solution of 0.15 mM **4a** (0.1 M [^{n}Bu$_4$N][ClO_4] in CH_3CN) produced a catalytic wave at a potential close to the position of $E^{\circ\prime}(Co^{II/I})$ for **4a**. At low acid concentrations, the catalytic wave had a peak-like shape, but for higher acid concentrations the current approached a plateau at potentials more negative than $E^{\circ\prime}(Co^{II/I})$. The potential at which catalysis took place remained nearly constant with increasing acid concentration. No catalytic waves were observed at potentials near the $E^{\circ\prime}(Co^{III/II})$, consistent with the fact that this potential was significantly more positive than the thermodynamic potential for hydrogen evolution using tosic acid as the proton source (vide infra). Similar behavior was observed when HBF_4·Et_2O was used as the proton source (Figure S1, Supporting Information). Hence, complex **4a** is a catalyst for electrochemical H_2 evolution in acidic CH_3CN solutions, and the catalysis is associated with reduction of the Co(II) complex to its Co(I) state.

Complex **4b** was also found to catalyze electrochemical H_2 evolution in acidic CH_3CN solutions, when either TsOH·H_2O or HBF_4·Et_2O was the acid. As for **4a**, the CV (Figure S2) showed that the catalysis by **4b** occurred at the $Co^{II/I}$ potential.

The CV of **5a** and **5b** in CH_3CN solutions did not vary upon addition of TsOH·H_2O. However, catalytic proton reduction was observed when HBF_4·Et_2O ($pK_a = 0.1$)[21,22] was used as the proton source (Figure S3). This behavior suggests that the proton activity obtained with TsOH·H_2O ($pK_a = 8.0$)[22,23] is not high enough to produce dihydrogen from the Co(I) forms of complexes **5a** and **5b**. Complexes **6a** and **6b** were also probed for electrochemical hydrogen evolution, but no catalysis was observed using either TsOH·H_2O or HBF_4·Et_2O as the acid source. In addition, no catalysis was observed for complexes **4a**−**6b** when the weak acid CF_3COOH ($pK_a = 12.7$)[22,23] was used as the acid source.

2.4. Stability of Co Macrocyclic Tetraimine Complexes in the Presence of Acid. The stability of **4a**−**5b** in the presence of excess acid was evaluated by electronic absorption spectroscopy (monitored at ∼400 nm for **4a** and **5a**, and ∼270 nm for **4b** and **5b**). These complexes showed negligible degradation over a period of several days in the presence of a 25-fold excess of TsOH·H_2O (10 mM), suggesting that these complexes are more acid tolerant than **1** and **2**. Under the same conditions, **1** degraded ∼10% in 1 h and **2** degraded ∼10% in 4 h. Complexes **4a**−**5b** degraded in the presence of excess HBF_4·Et_2O but more slowly than **1** and **2**. For example, **4a** and **4b** degraded only 5% in 2 h in the presence of a 30-fold excess of HBF_4·Et_2O (3 mM), while under the same conditions **1** and **2** degraded completely within minutes.[10] The Co(II) complexes $[Co^{II}(Tim^{Me})(CH_3CN)_2]^{2+}$ (**4c**) and $[Co^{II}(Tim^{Me/Ph})(CH_3CN)_2]^{2+}$ (**5c**) had stabilities that were similar to those for **4b** and **5b**, respectively.

2.5. Catalytic Efficiency of Co Tetraimine Complexes for H_2 Evolution as Determined by Bulk Electrolysis. Previous bulk electrolysis experiments indicated that the catalytic currents observed by cyclic voltammetry for complexes **1** and **2** were associated with electrocatalytic evolution of H_2, with approximately quantitative faradaic yields for H_2 production. Turnover numbers (TNs) were >5 (TN = moles of hydrogen produced divided by moles of catalyst used) were observed, without appreciable decomposition of the catalysts.[10] To evaluate the behavior of the Co tetraimine complexes, analogous bulk electrolysis experiments were performed with solutions of **4a**−**5b** (Table 1). During bulk electrolysis potentials were applied at −0.58 V (for **4a**−**b**) or −0.48 V (for **5a**−**b**) vs SCE. Solutions that contained an excess of acid and catalysts **4a**−**5b** turned from green to red-purple upon electrolysis. This behavior suggested that under such conditions the catalyst was reduced to its Co(II) form, $[Co^{II}(Tim^{Me})(CH_3CN)_2]^{2+}$ (**4c**) or $[Co^{II}(Tim^{Me})(CH_3CN)_2]^{2+}$ (**5c**).[19] The CV of **4c** and **5c** was identical to that of **4b** and **5b**.

When a cobalt complex having a Tim^{Me} ligand (**4a**−**4c**) was used in bulk electrolysis experiments, H_2 was produced (as determined by GC−MS) in quantitative faradaic yields (Table 1). After five turnovers, no deactivation of the catalyst was observed. However, when a cobalt complex having the $Tim^{Me/Ph}$ ligand (**5a**−**5c**) was used as the catalyst, the faradaic yield for H_2 production was only 20−25%. After two turnovers, appreciable deactivation of the catalyst was observed. The lower faradaic yields observed for **5a**−**5c** most likely reflect the decomposition of intermediate species during the course of electrolysis, rather than the acid sensitivity of the precatalysts, since **5a**−**5c** are in fact somewhat more stable in the presence of an excess of acid than are **4a**−**4c**.

2.6. Kinetic and Mechanistic Analysis. CV data for complexes **1**, **2**, **4a**, and **4b** were obtained as a function of acid and catalyst concentrations.[24] The CV of the catalysts, with no added acid, had well-defined reversible $Co^{II/I}$ reductions (peak separations of 80 ± 10 mV). The potentials for all the complexes are shown in Table 2. The diffusion coefficient for each catalyst,

(21) Assuming etherated HBF_4 completely dissociates into etherated proton and BF_4^- in acetonitrile, its pK_a roughly equals the pK_a for diethyl ether (as base), which is 0.1. See ref 22.
(22) Izutsu, K. *Acid-Base Dissociation Constants in Dipolar Aprotic Solvents*; Blackwell Scientific Publications: Oxford, 1990.
(23) All pK_a values cited in this paper were referred to pK_a's in acetonitrile.
(24) Due to the instability of **1** and **2** in the presence of a large excess of HBF_4-(Et_2O), and due to the nonunity faradaic yield for H_2 evolution by **5a** and **5b** in $HBF_4(Et_2O)$, the studies were performed using complexes **1**, **2**, **4a**, and **4b** and using TsOH(H_2O) as the acid.

Table 1. Summary of Bulk Electrolysis Results

complex	proton source	concn of catalyst (mM)	concn of acid (mM)	volume (mL)	potential (V vs SCE)	duration (min)	charge (coulomb)	faradaic yield for H_2 (%)
4a	$TsOH·H_2O$	0.9	21	100	−0.58	30	49	∼90
4b/4c	$TsOH·H_2O$	0.8	22	100	−0.58	30	54	∼100
5a	$HBF_4·Et_2O$	0.9	20	100	−0.48	30	15	∼20
5b/5c	$HBF_4·Et_2O$	0.7	20	100	−0.48	30	16	∼25

Table 2. Reduction Potentials, Apparent Rate Constants, and Diffusion Constants for Cobalt Complexes

complex	$E^{o\prime}$(Co(III/II) (V vs SCE)	$E^{o\prime}$(Co(II/I)) (V vs SCE)	$k_{app} \times 10^{2}$ [d] (M^{-1} s^{-1})	$D \times 10^{5}$ [e] cm^2/s
1	∼0.2[a]	−0.55	7 × 10[e]	0.8
2	∼0.3[a]	−0.28	2	0.14
4a	−0.06[b]	−0.38	4	2.5
4b	NO[c]	−0.35	3	1.2
5a	−0.03[b]	−0.25	NA	
5b	NO[c]	−0.20	NA	
6a	0.03[b]	−0.15	NA	
6b	NO[c]	−0.08	NA	

[a] Irreversible couple. [b]Reversible couple. [c]Not observed. [d] $TsOH·H_2O$ was used as the proton source; rates obtained from eq 1, $n = 2$, $S = 0.07$ cm^2. [e]Diffusion constant determined by simulation of CV in absence of acid.

determined by simulation of its CV in the absence of acid, is shown in Table 2.

The overall rate constant for H_2 evolution may be estimated from the height of the catalytic plateau current at high overpotentials.[14,15] A plateau shape is only observed when the rate of the reduction of the catalytic species at the electrode is equal to the rate of its reoxidation by the acid. Additionally, the acid concentration in the reaction region must not be depleted.[14,15] Under these conditions, for a reaction that is first order in both catalyst and acid, the value of the current in the plateau region is given by

$$i_c = nFSC_p^{\circ}(DkC_s^{\circ})^{1/2} \quad (1)$$

where n is the number of electrons, i_c is the plateau current (mA), F is Faraday's constant (96 485 C mol^{-1}), S is the area of the electrode surface (cm^2), C_p° is the bulk concentration of redox active species (M), D is the diffusion coefficient (cm^2 s^{-1}), k is the reaction rate constant (M^{-1} s^{-1}), and C_s° is the bulk concentration of acid (M).[14,15]

The dependence of i_c on the concentrations of catalyst and acid was measured for the complexes. For H_2 evolution catalyzed by **1** or **4a** using $TsOH·H_2O$ as the acid, the catalytic waves did not exhibit, but approached, a plateau shape under certain conditions. The peak values of such catalytic currents were taken as approximations for the values of the plateau currents. As shown in Figure 6, for catalysis by **1**, the catalytic rate was found to be first order in the concentration of acid and less than first order in the concentration of catalyst. For catalysis by **4a**, the catalytic rate was found to be first order in the concentrations of both acid and catalyst (Figure S4).

The catalytic waves reached a plateau shape using **2** or **4b** as the H_2 evolution catalyst when the concentration of $TsOH·H_2O$ was much larger than that of the catalyst. In these cases, the catalytic rate followed a first-order dependence on the concentration of both acid and catalyst (Figures S5−S6). Approximate catalytic rate constants, k_{app}, with $TsOH·H_2O$ were obtained using eq 1 (Table 2).

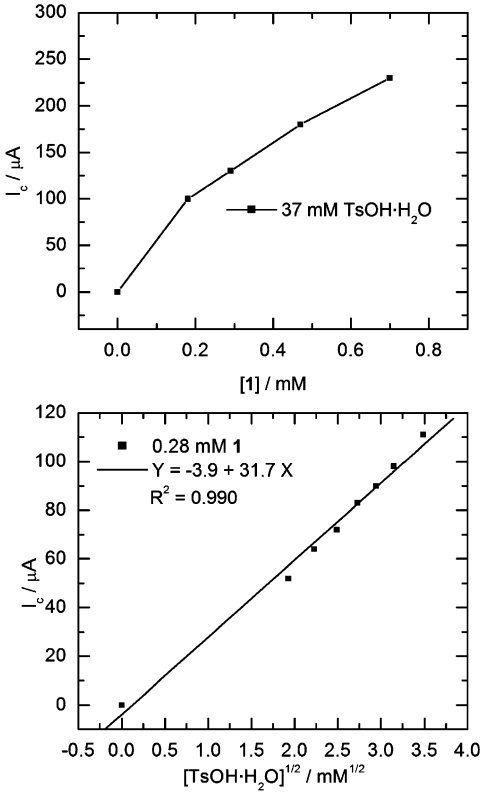

Figure 6. Dependence of the catalytic plateau current, i_c, on the concentrations of catalyst (top) and acid (bottom) for complex **1**; $TsOH·H_2O$ was used as the acid, with a scan rate of 100 mV/s and $S = 0.07$ cm^2. In the plots the plateau current was set to zero in the absence of acid, as predicted by eq 1, even though the catalyst has a nonzero *peak* current under such conditions.

Digital simulations of the cyclic voltammetric data were performed to study the mechanism of electrocatalytic H_2 evolution for complexes **1**, **2**, **4a**, and **4b**. The CV was simulated assuming either a monometallic or a bimetallic mechanism (Scheme 3) for H_2 formation.

For catalysis by **1**, when a monometallic mechanism (eqs 2−6) was assumed, it was not possible to use a common set of parameters to simulate the CV for a given concentration of catalyst in the presence of incremental amounts of $TsOH·H_2O$. The simulated currents increased with acid ($TsOH·H_2O$) much more rapidly than observed experimentally. In addition, the simulated CV maintained its peak-type shape at all concentrations of acid used experimentally, while the experimental CV approached a plateau shape as the acid concentration increased. Hence, electrocatalytic H_2 evolution by **1** is *not* dominated by a simple monometallic mechanism.

Simulation of the CV for catalyst **1** assuming a bimetallic mechanism (eqs 2−4 and 7) gave rise to a more satisfactory simulation of the experimental data for a given concentration

Scheme 3. Two Mechanistic Pathways for Electrochemical Proton Reduction Catalyzed by Cobalt Macrocyclic Complexes

Electron Transfer:	$Co(III) + e^- \rightarrow Co(II) \quad E^{0'}(Co^{III/II})$	(2)
	$Co(II) + e^- \rightarrow Co(I) \quad E^{0'}(Co^{II/I})$	(3)
Hydride Formation:	$Co(I) + HA \rightarrow Co(III)\text{-}H + A^- \quad K_4, k_4$	(4)
Monometallic Pathway	$Co(III)\text{-}H + HA \rightarrow Co(III) + H_2 + A^- \quad K_5, k_5$	(5)
	$Co(III) + Co(I) \rightarrow 2\ Co(II) \quad K_6, k_6$	(6)
Bimetallic Pathway	$Co(III)\text{-}H + Co(III)\text{-}H \rightarrow 2\ Co(II) + H_2 \quad K_7, k_7$	(7)

of catalyst in the presence of incremental amounts of $TsOH\cdot H_2O$ (Figures S7 and S8). However, for different concentrations of catalysts, the rate constants obtained were different. At lower catalyst concentration larger rate constants were obtained ([**1**] = 0.22 mM; $k_4 = 1.5 \times 10^5\ M^{-1}\ s^{-1}$, $k_7 = 1.5 \times 10^6\ M^{-1}\ s^{-1}$) than at higher catalyst concentration ([**1**] = 1.0 mM; $k_4 = 7 \times 10^3\ M^{-1}\ s^{-1}$, $k_7 = 9 \times 10^5\ M^{-1}\ s^{-1}$) (Figures S7 and S8).

The changes in calculated rate constants with catalyst concentration are consistent with Figure 6, which suggests that the catalysis by **1** is less than first order in catalyst. Therefore the CV data indicate that the production of H_2 most likely proceeds by a bimetallic pathway; however, direct kinetic evidence to support this conclusion is needed.

For catalysis by **4a**, a monometallic mechanism was also ruled out because simulations indicated that a monometallic pathway would give rise to catalytic waves for the oxidation of H_2 by Co(III) (step 5) at the $Co^{III/II}$ potential. These oxidative catalytic currents were not observed in our experiments. On the other hand, a bimetallic mechanism with the same set of rate constants can be used to simulate the catalytic waves from two different concentrations of catalyst in the presence of incremental amounts of acid (Figures S9 and S10).

For catalysis by **2** and **4b**, the catalytic waves can be crudely simulated using either a monometallic or a bimetallic mechanism. Simulation itself therefore does not distinguish between these two mechanisms without prior knowledge of the equilibrium constants and/or reaction rates of the key chemical steps (Figures S11−S14).

2.7. Evidence for a Cobalt(III) Hydride Intermediate. In the presence of $TsOH\cdot H_2O$, a quasi-reversible redox wave for complex **1** was observed when the potential was scanned negative of $E^{\circ\prime}(Co^{II/I})$ (Figure 7); however, no catalytic wave was observed at this reduction potential. In the absence of acid, no such wave was observed. We tentatively assign this wave to the "Co(III)−H"/"Co(II)−H" redox couple produced by the putative $[HCo(CH_3CN)(dmgBF_2)_2]$ intermediate formed in situ upon reduction of **1** in the presence of acid (see discussion). The electrochemistry of course cannot distinguish between a cobalt or ligand centered reduction of the Co(III)−H.

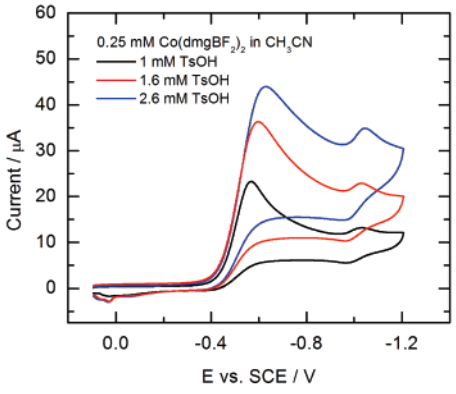

Figure 7. Cyclic voltammogram of **1** in the presence of acid showing a redox couple assigned as Co(III)−H/Co(II)−H; the scan rate was 100 mV/s.

No reversible redox wave for a Co(III)−H/Co(II)−H couple was observed for **2**. Instead, a catalytic wave was observed at a potential of −0.85 V vs SCE, i.e., 570 mV more negative than the value of $E^{\circ\prime}(Co^{II/I})$ for **2** (Figure S15).

Redox waves for the Co(III)−H/Co(II)−H couple were also observed for **4a**−**b** (Figure S16). In contrast, for complexes **5a**−**b** in the absence of acid, at potentials close to those expected for the Co(III)−H/Co(II)−H couples, redox waves were observed. This reduction of a Co(I) species is likely a ligand-centered redox process. The intermediacy of a Co(III)−H could therefore not be ascertained from the cyclic voltammetric data for these two complexes.

2.8. Hydrogen Oxidation. We have studied the cobalt complexes **1** and **2** to determine their ability to electrocatalytically *oxidize* hydrogen under 1 atm of H_2 in CH_3CN solutions buffered with either $[^nBu_4N][CF_3CO_2]$ (for **1**) or $[^nBu_4N][TsO]$ (for **2**). No oxidation activity could be detected at scan rates between 100 and 1000 mV per second near the Co(II/I) potential; however, we observed that H_2 was oxidized by **1** in the presence of $[^nBu_4N][CF_3CO_2]$ in CH_3CN over a period of several days, reaching an equilibrium mixture represented by eq 8 (Figure 8).

$$[Co^{II}(dmgBF_2)_2(CH_3CN)_2] + {}^1/_2H_2 + [NBu_4][CF_3CO_2] \leftrightarrow CF_3COOH + [Co^{I}(dmgBF_2)_2(CH_3CN)][NBu_4] + CH_3CN \quad (8)$$

As shown in Figure 8, when 1 atm of H_2 was initially added to a solution of 1.6 mM **1** in the presence of 66 mM $[NBu_4][CF_3CO_2]$, the solution maintained its yellow color, indicative of the $[Co^{II}(dmgBF_2)_2(CH_3CN)_2]$ species in solution. With time, the solution gradually turned dark blue, indicative of the formation of $[Co^{I}(dmgBF_2)_2(CH_3CN)]^-$ in the reaction medium. After 34 h, the reaction reached equilibrium, and the concentrations of $[Co^{II}(dmgBF_2)_2(CH_3CN)_2]$ (0.55 mM) and $[Co^{I}(dmgBF_2)_2(CH_3CN)]^-$ (1.05 mM) were determined using their extinction coefficients at 630 nm (for Co(I)) and 440 (for Co(II)).[10] The absence of isosbestic points in Figure 8 suggests the possibility that some degradation occurs over prolonged periods of time under these conditions, perhaps due to side reactions that reduce the

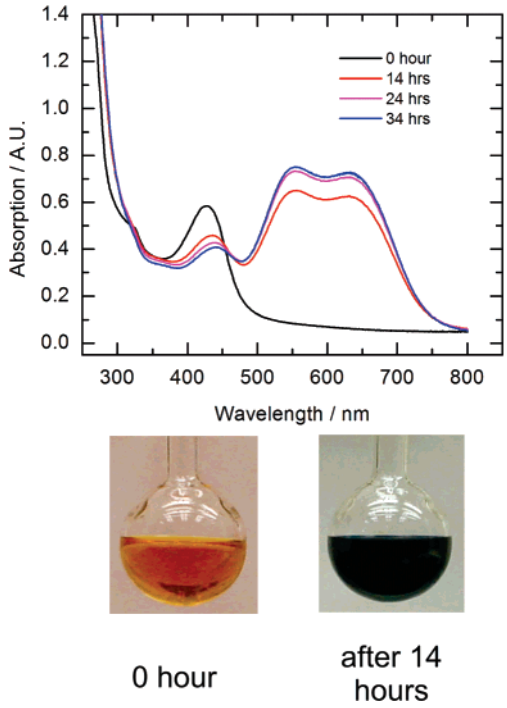

Figure 8. Time-dependent UV−vis spectra (top) and pictures (bottom) of solutions initially containing 1.6 mM of $Co(dmgBF_2)_2$ (**1**), 66 mM $[NBu_4][CF_3CO_2]$, and 1 atm of H_2.

unsaturated ligand backbone. The equilibrium constant for eq 8 is approximated to be 0.03 $atm^{-1/2}$, corresponding to an overpotential of approximately 90 mV for H_2 evolution by catalyst **1**. We were not able to observe similar H_2 oxidation by **2** in the presence of $[^nBu_4N][TsO]$ in CH_3CN over a few weeks, indicating that H_2 oxidation by **2** was appreciably slower.

3. Discussion

3.1. Structural Aspects of Co Diglyoxime Complexes. Complex **2** is the only crystallographically characterized cobalt(II) complex with the $(dpgBF_2)_2$ ligand. The salient features of its structure are similar to those of $Co(dmgBF_2)_2(CH_3OH)_2$, which has an average Co−N(imine) distance of 1.876(4) Å and a Co−O(CH_3OH) distance of 2.264(4) Å.[25]

Complex **3** is the only crystallographically characterized cobalt(I) complex of the $(dpgBF_2)_2$ ligand. In general, structurally characterized cobalt(I) complexes with macrocyclic imine ligands are rare. Espenson and co-workers reported the structurally related complex $[Co(dmgBF_2)_2(py)][^nBu_4N]$, in which the Co(I)−N(imine) bond has an average distance of 1.839(3) Å, also shorter than the corresponding bond (1.878(4) Å) in its Co(II) analogue.[26] The bond contraction was also attributed to a higher degree of π-back-bonding in the cobalt(I) complex.[26] The cobalt(I) center is displaced 0.26 Å toward the pyridine ligand above the macrocyclic plane of the $(dmgBF_2)_2$ ligand.

3.2. Mechanistic Aspects of Electrocatalytic H_2 Evolution from the Cyclic Voltammetric Behavior of Co Macrocycles. The electrochemistry of **1** and **2** (Scheme 1) had been previously investigated in the presence of CF_3COOH (pK_a = 12.7 in CH_3CN),[21,22] $HCl{\cdot}Et_2O$ (pK_a = 8.9), and $HBF_4{\cdot}Et_2O$ (pK_a = 0.1).[21−23] Catalytic waves were observed corresponding to hydrogen evolution near the value of $E^{\circ\prime}(Co^{II/I})$ (−0.55 V for **1** and −0.28 V for **2** in CH_3CN vs SCE), using $HBF_4{\cdot}Et_2O$, $HCl{\cdot}Et_2O$, and CF_3COOH as the acids for **1**, and $HBF_4{\cdot}Et_2O$ and $HCl{\cdot}Et_2O$ as the acids for **2**.[10] The presence of a large excess of coordinated chloride anion had a profound influence on the shape and position of the observed catalytic waves when $HCl{\cdot}Et_2O$ was used as the acid. Thus we have used *p*-toluenesulfonic acid ($TsOH{\cdot}H_2O$, pK_a = 8.0) in this study,[22,23] which is similar in acid strength to $HCl{\cdot}Et_2O$, but features a much more weakly coordinating counteranion.

A clear correlation was observed between the activity toward H_2 evolution and the $Co^{II/I}$ potentials of the catalysts, with those complexes having more negative $Co^{II/I}$ potentials being more active. For the cobalt catalysts investigated here, the complex with the most negative $Co^{II/I}$ reduction potential, **1**, mediated H_2 evolution using the weakest acid CF_3COOH (pK_a = 12.7),[10] while the complexes with more positive potentials, **2**, **4a**, and **4b**, required stronger acids, such as $TsOH{\cdot}H_2O$ (pK_a = 8.0). The complexes with the most positive potentials, **5a** and **5b**, required an even stronger acid, such as $HBF_4{\cdot}Et_2O$ (pK_a = 0.1). For complexes that are more readily reduced than **5b**, such as **6a** and **6b**, no catalysis was observed even with $HBF_4{\cdot}Et_2O$ as the acid. When using the same acid, the more negative the $Co^{II/I}$ potential, the faster the catalysis (Table 2). These observations reflect that the basicity of the active Co(I) species is related to its $Co^{II/I}$ redox potential. A similar trend has been observed by Collman and co-workers for cofacial bis(alkyl) diporphyrin complexes that also catalyze H_2 evolution, but at much more negative potentials (−1.2 to −1.8 V vs SCE) than those for the Co macrocycles investigated here.[5] The more easily reduced diporphyrin complexes produced H_2 at more positive potentials but required stronger acids to achieve reasonable reaction rates.[5]

For the electrocatalysts examined here, H_2 evolution occurred at potentials just negative of the $E^{\circ\prime}(Co^{II/I})$ values for the complexes. Thus H_2 production required prior generation of the Co(I) species. This conclusion is in accord with that of Espenson and co-workers, who studied the evolution of H_2 using $Co(dmgBF_2)_2(H_2O)_2$ as the catalyst, $CrCl_2$ as the electron donor, and HCl(aq) as the proton source.[11] Stopped-flow kinetics experiments in that system allowed identification of a chloride-bridged complex $[(H_2O)_5Cr{-}Cl{-}Co(dmgBF_2)_2]^+$ as an intermediate. This intermediate was suggested to decompose to a cobalt(I) species $[LCo(dmgBF_2)_2]^-$, which thereafter reacted with a proton to form a cobalt(III) hydride, $[H{-}Co(L)(dmgBF_2)_2]$.[11] The Co(III) hydride was presumed to react further to produce H_2. Two mechanisms were considered: one that involved the protonation of the hydride ligand to produce H_2, and the other involving a bimetallic reaction of two Co(III) hydrides.[11]

Similar mechanisms can be envisioned for electrocatalytic H_2 evolution by the catalysts **1**−**2** and **4a**−**5b**, except that the active Co(I) species is generated electrochemically (Scheme 3). The CV of the $Co^{II/I}$ couples, with no added acid, was electrochemically reversible. Thus the rates of interfacial electron transfer from the electrode to the Co(II) catalysts are faster than

(25) Bakac, A.; Brynildson, M. E.; Espenson, J. H. *Inorg. Chem.* **1986**, *25*, 4108−4114.
(26) Shi, S.; Daniels, L. M.; Espenson, J. H. *Inorg. Chem.* **1991**, *30*, 3407−3410.

the rate of diffusion of the Co(II) species to the electrode surface.[14] The electrocatalysis differs from the chemical catalysis because the reduction of the Co(II) by chromous ion is slow ($k \approx 0.25\ s^{-1}$ for generation of $[Co(dmgBF_2)_2]^-$ from $[(H_2O)_5Cr-Cl-Co(dmgBF_2)_2]^+$)[11] and rate limiting for H_2 evolution. The electrochemical H_2 evolution studied here in CH_3CN is much more rapid.

The presumed Co(III)−H complexes that are formed upon protonation of the Co(I) can in principle be further reduced to form Co(II)−H species, which could go on to produce H_2. We have not been able to synthesize a genuine Co(III)−H complex with $(dmgBF_2)_2$, $(dpgBF_2)_2$, or Tim^R (R = Me, Me/Ph, and Ph) as the supporting ligand. Protonation of the Co(I) species with tosic acid, CF_3COOH, or anisidinium ($pK_a = 11.8$)[22] gave Co(II) complexes with the corresponding ligands, with no evidence for the formation of a long-lived cobalt(III)−H species. Likewise, reduction of the Co(III) halide complexes with $NaBH_4$ or $NaEt_3BH$ gave similar Co(II) products. This would be consistent with a Co(III)−H species that can bimolecularly release H_2 at a rate that precludes its isolation (eq 7 in Scheme 3). The potentials for reported $Co^{III/II}$ couples of cobalt(III) alkyl complexes $RCo(dmgBF_2)_2(H_2O)$ (R = CH_3, C_2H_5, *n*-C_3H_7) are −1 V vs SCE.[27] We expect that the potential for the $Co^{III/II}$ couple of cobalt(III) hydride complexes, $HCo(dmgBF_2)_2(L)$, should be similar to that of $RCo(dmgBF_2)_2L$ and be significantly more negative than $E^{\circ\prime}(Co^{II/I})$ for the parent $Co(dmgBF_2)_2(L)_2$. Because electrocatalysis occurs near the measured value of $E^{\circ\prime}(Co^{II/I})$ for all of the catalysts studied here, the intermediacy of a Co(II)−H species seems highly unlikely. More negative potentials, however, could facilitate a pathway for H_2 evolution that is mediated by a Co(II)−H species.

Scheme 3 shows two limiting reaction pathways for the formation of H_2 from a cobalt(III) hydride. The measured potentials for the reductions of the $Co^{III/II}$ and $Co^{II/I}$ couples (eqs 2 and 3) along with the H_2 evolution potential[22,28−30]

$$HA + e^- \rightarrow {}^1/_2H_2 + A^- \qquad E^{\circ\prime}(HA) \tag{9}$$

yield the equilibrium constant for the following monometallic reaction:

$$Co(I) + 2\ HA \rightarrow Co(III) + H_2 + 2A^- \qquad K_{mono} \tag{10}$$

We obtain

$$eq(10) = 2 \times eq(9) - eq(2) - eq(3) \tag{11}$$

and

$$K_{mono} = \exp\left\{\frac{e(2E^{\circ\prime}(HA) - E^{\circ\prime}(Co^{III/II}) - E^{\circ\prime}(Co^{II/I}))}{k_BT}\right\}$$
$$= \exp\left\{\frac{e[(E^{\circ\prime}(HA) - E^{\circ\prime}(Co^{III/II})) + (E^{\circ\prime}(HA) - E^{\circ\prime}(Co^{II/I}))]}{k_BT}\right\} \tag{12}$$

where e is the charge on the electron, k_B is the Boltzmann constant, and T is the temperature. The values of $E^{\circ\prime}(HA)$ have been estimated as −0.51, −0.23 and +0.23 V vs SCE for CF_3COOH, $TsOH\cdot H_2O$, and $HBF_4\cdot Et_2O$, respectively (vide infra).[28,29]

Table 3. Equilibrium Constants for the Reduction of an Acid by the Co(I) Complexes

acid		pK_{mono}	pK_{bi}
CF_3COOH	**1**	−11.3	1.4
$TsOH\cdot H_2O$	**1**	−1.9	10.8
$HBF_4\cdot Et_2O$	**1**	13.7	26.4
CF_3COOH	**2**	−17.6	−7.8
$TsOH\cdot H_2O$	**2**	−8.1	1.7
$HBF_4\cdot Et_2O$	**2**	7.4	17.2
CF_3COOH	**4a**	−9.9	−4.4
$TsOH\cdot H_2O$	**4a**	−0.34	5.1
$HBF_4\cdot Et_2O$	**4a**	15.2	20.6

The equilibrium constant for the bimetallic pathway can also be estimated in a similar manner with

$$2Co(I) + 2\ HA \rightarrow 2Co(II) + H_2 + 2A^- \qquad K_{bi} \tag{13}$$

$$eq(13) = 2 \times eq(9) - 2 \times eq(3) \tag{14}$$

and

$$K_{bi} = \exp\{2e(E^{\circ\prime}(HA) - E^{\circ\prime}(Co^{II/I}))/k_BT\} \tag{15}$$

Calculations for the mono and bimetallic equilibrium constants are shown in Table 3 for CF_3COOH, $TsOH\cdot H_2O$, and $HBF_4\cdot Et_2O$. For complex **1** and **2** the monometallic reduction of acid, K_{mono} is very unfavorable, except in the presence of the strongest acid $HBF_4\cdot Et_2O$. However, K_{bi} is generally favorable except for complexes **2** and **4a** with the weakest acid, CF_3COOH.

The complete reaction for the reduction of acid by the Co(I) complex for either pathway is given by eq 13. For the monometallic pathway, the reduction of the acid by Co(I), eq 10, must be driven by the comproportionation reaction of Co(III) produced in eq 10 with Co(I). It seems unlikely that a very unfavorable equilibrium constant of less than 1×10^{-10} can be compensated by the reduction of Co(III). The monometallic pathway is only likely to be important for very strong acids and/or complexes with a relatively negative Co(III/II) potential. A similar argument has been made by Spiro et al. to rule out a monometallic mechanism in a cobalt catalyzed hydrogen evolution system.[31]

The kinetics of the bimetallic pathway can be derived using a steady state approach (see Supporting Information for details). Two limiting rate laws result. One applies when the protonation step (eq 4) is fast:

(27) Shi, S.; Bakac, A.; Espenson, J. H. *Inorg. Chem.* **1991**, *30*, 3410−3414.
(28) Felton, G. A. N.; Glass, R. S.; Lichtenberger, D. L.; Evans, D. H. *Inorg. Chem.* **2006**, *45*, 9181−9184.
(29) We chose a potential of −0.14 V vs Fc/Fc^+ (i.e., 0.24 V vs SCE using $[^nBu_4](ClO_4)$ as the electrolyte, see ref 30) as the thermodynamic potential for H^+/H_2 in acetonitrile. This potential was determined by Daniele, S., et al. using platinized platinum as the working electrode. A reversible H^+/H_2 couple was observed in acetonitrile, and the potential for this couple corresponds to the true thermodynamic potential for this reaction. It is noted, however, that Parker, V. D., et al. (*Acc. Chem. Res.* **1993**, *26*, 287−294) and DuBois, D. L., et al. (*J. Am. Chem. Soc.* **2004**, *126*, 2738−2743) estimated values of −0.05 V and −0.07 V vs Fc/Fc^+, respectively, for H^+/H_2 in acetonitrile, based on the junction potential between aqueous and acetonitrile solutions.
(30) Connelly, N. G.; Geiger, W. E. *Chem. Rev.* **1996**, *96*, 877−910.
(31) Kellett, R. M.; Spiro, T. G. *Inorg. Chem.* **1985**, *24*, 2373−2377.

$$Rate = K_4^2 k_7 \left[\frac{[\mathrm{Co(I)}][\mathrm{HA}]}{[\mathrm{A}^-]}\right]^2$$

This rate law requires a second-order dependence on the concentrations of Co(I) and acid and an inverse second-order dependence on the concentration of the conjugate base of the acid. The square of the equilibrium constant appears as would be expected for a rapid pre-equilibrium. Our electrochemical data do not support this rate law since a first-order dependence on cobalt and acid is observed, except for complex **1** where the dependence on cobalt was less than first order. The second limiting scenario occurs when the formation of Co(III)−H is rate limiting (eq 4) and the subsequent reactions are fast. For this case we obtain

$$Rate = k_4[\mathrm{Co(I)}][\mathrm{HA}]$$

The rate is first order in both acid and cobalt, and only the kinetics of the formation of the hydride are important. This case is consistent with most of the observations.

Digital simulation of the cyclic voltammetric data[32] was used to study the mechanism of the H_2 evolution catalysis. The simulations suggest that catalysis by **1** and **4a** proceeds, at least predominantly, through a bimetallic mechanism. This is consistent with the previous study by Espenson and co-workers on the mechanism of stoichiometric H_2 formation from a kinetically stabilized Co(III)−H species, $[HCo(P(^nBu)_3)(dmgH)_2]$ (dmgH = dimethygloxime) in the presence of acid.[33] Espenson's study suggested that H_2 was formed predominantly by the bimetallic mechanism (eq 7) with a rate constant of 1.7×10^4 M^{-1} s^{-1}; however, H_2 was also formed by protonation of $[HCo(P(^nBu)_3)(dmgH)_2]$ (eqs 5 and 6), albeit with a much lower rate constant of 0.42 M^{-1} s^{-1}. Simulations were not able to distinguish the bimetallic and monometallic pathways for catalysis by **2** and **4b**.

After submission of this manuscript, a related study by Artero et al. on the electrocatalytic H_2 evolution by **1** appeared.[34] Their simulation studies led them to conclude that H_2 evolution proceeded via a *monometallic* mechanism at the $Co^{II/I}$ potential when the *p*-cyanoanilinium cation ($pK_a = 7.6$ in CH_3CN)[22] was used as the proton source. The bimetallic mechanism was ruled out by the authors based on the fact that it could not be simulated to fit the data obtained using different acids (CF_3COOH, *p*-cyanoanilinium, and Et_3NH). Surprised by the discrepancy between our electrochemical conclusions using tosic acid and those of Artero and co-workers using *p*-cyanoanilinium, we undertook an independent evaluation of H_2 evolution catalysis by **1** using *p*-cyanoanilinium as the acid in our lab. When collected under the same conditions as those reported by Artero et al., our experimental data were consistent. Additionally, we examined the electrocatalysis with an acid/catalyst ratio larger than 10, which was not presented in Artero's paper (Figures S17−18). We found that both the monometallic and bimetallic mechanisms can be used to satisfactorily simulate the experimental data when the acid/catalyst ratio is ca. 10 or less. However, only by assuming a bimetallic mechanism can the simulated catalytic waves match the experimental waves collected over the entire range of acid/catalyst ratios (1/1−40/1), in terms of both current height and shape (Figures S17−18). These observations, together with the thermodynamic considerations outlined in the previous paragraphs, lead us to conclude that the bimetallic pathway is the dominant H_2 evolution pathway catalyzed by **1** using *p*-cyanoanilinium, $TsOH\cdot H_2O$, or CF_3COOH as the acid. Direct studies of the chemical kinetics of the H_2 evolution catalysis is warranted to further elucidate the mechanistic details.

3.3. Observation of Co(III)−H Intermediates in H_2 Evolution. Evidence for a cobalt(III)−hydride intermediate was obtained by the observation of a nearly reversible Co(III)−H/Co(II)−H couple ($E^{\circ\prime} \approx -1.0$ V vs SCE) for the $[HCo(CH_3CN)(dmgBF_2)_2]$ intermediate species formed *in situ* upon reduction of the Co(II) species in the presence of acid (Figure 7). As mentioned above the $E^{\circ\prime}$ value for this redox wave is close to the $E^{\circ\prime}$ position of −1.1 V vs SCE that has been observed for various $RCo(dmgBF_2)_2(H_2O)$ (R = CH_3, C_2H_5, n-C_3H_7) complexes.[27]

When the catalysis at the $Co^{II/I}$ potential of the original complex is rapid and the concentration of acid is not too large, the concentrations of acid and Co(III)−H in the reaction layer near the electrode at the Co(III)−H/Co(II)−H potential will be low. Therefore, only small amounts of Co(II)−H are formed at steady state. The Co(II)−H would then react only slowly due to the low concentrations of Co(II)−H and acid. This would enable a reoxidation wave for what is presumably an even more reactive Co(II)−H species to be observed, as shown in Figure 7. Similar observations have been made by Artero et al. on H_2 evolution catalysis by **1** using a *p*-cyanoanilinium salt as the acid.[34]

No reversible redox wave for a Co(III)−H/Co(II)−H couple could be observed for **2**. Rather, a catalytic wave was observed at a potential ∼570 mV more negative than those for the $Co^{II/I}$ potential. This catalytic wave can be attributed to electrocatalytic H_2 evolution by a Co(II)−H species $[HCo(CH_3CN)(dpgBF_2)_2]^-$, which can be alternatively formulated as a cobalt(III) hydride species with a ligand radical anion. Because the catalysis for **2** is slow at the $E^{\circ\prime}(Co^{II/I})$ potential, the concentrations of the $[HCo(CH_3CN)(dpgBF_2)_2]$ intermediate and acid in the reaction layer are presumably large enough to trigger a catalytic wave at the Co(III)−H/Co(II)−H potential. Thus no reoxidation wave for $[HCo(CH_3CN)(dpgBF_2)_2]^-$ was observed. Artero et al. observed a similar catalytic wave at the Co(III)−H/Co(II) potential for **1** using a very weak acid, Et_3NHCl as the acid in CH_3CN ($pK_a = 18.7$).[22,34]

Quasi-reversible redox waves for the Co(III)−H/Co(II)−H couple could be observed for **4a**−**b** because the catalysis at $Co^{II/I}$ potentials for **4a**−**b** is efficient and hence the concentrations of $[HCo(Br)(Tim^{Me})]^+$ intermediates and of acid are small in the reaction layer at the Co(III)−H/Co(II)−H potential. The cyclic voltammetric scan is again fast enough to reoxidize Co(II)−H prior to its reaction with either the acid or itself.

These observations of redox/catalytic waves associated with Co(III)−H/Co(II)−H couples in the H_2 evolution catalysis by complexes **1**−**2** and **4a**−**b** provide evidence for the intermediacy of Co(III) hydride species in the electrocatalysis and help to validate eq 4 in Scheme 3. This study can also be compared to that of Saveant and co-workers on H_2 evolution catalyzed by an iron porphyrin complex (tetraphenylporphyrin)FeCl.[6] The intermediacy of an Fe(II) hydride species was proposed in their

(32) Rudolph, M. *DigiElch 2.0*. http://www.digielch.de/.
(33) Chao, T. H.; Espenson, J. H. *J. Am. Chem. Soc.* **1978**, *100*, 129−133.
(34) Baffert, C.; Artero, V.; Fontecave, M. *Inorg. Chem.* **2007**, *46*, 1817−1824.

study due to the appearance of a nearly reversible redox wave at −1.88 V vs SCE, 280 mV more negative than the $E^{\circ\prime}$ value for the catalytically active $Fe^{I/0}$ couple. Similar to the present system, the $E^{\circ\prime}$ potential for the Fe(II)−H/Fe(I)−H couple was close to those of −1.95 V vs SCE found for the Fe(II)−R/Fe(I)−R couples, where R is a methyl or an ethyl group.

3.4. Overpotential for Hydrogen Evolution, Hydrogen Oxidation Activity, and Comparison between Low Overpotential Catalysts. The reduction potential for H_2 evolution, $E^{\circ\prime}(HA/H_2)$, from a solution of an acid HA, $HA + e^- = {}^1/_2H_2 + A$, varies with acid strength. The potential is related to the proton reduction potential, $E^{\circ\prime}(H^+/H_2)$ ($H^+ + e^- = {}^1/_2\ H_2$), by

$$E^{\circ\prime}(HA/H_2) = E^{\circ\prime}(H^+/H_2) - 0.059\ pK_a(HA)$$

$E^{\circ\prime}(H^+/H_2)$ is 0.24 V vs SCE in CH_3CN using $[^nBu_4N][ClO_4]$ as the electrolyte.[29,30] Thus, in CH_3CN, the value of $E^{\circ\prime}(HA/H_2)$ has been estimated to be −0.51, −0.23, and 0.23 V vs SCE for CF_3COOH, $TsOH\cdot H_2O$, and $HBF_4\cdot Et_2O$, respectively.[22,28,29,35] The complexes studied herein appear to catalyze H_2 evolution at measurable rates *close to* the reversible HA/H_2 potential, for a given acid in CH_3CN. The overpotential determined by electrochemistry is 40 mV using **1** as the catalyst and CF_3COOH as the acid and is 50 mV using **2** as the catalyst and $TsOH\cdot H_2O$ as the acid. We have studied the cobalt complexes **1** and **2** to determine their ability to electrocatalytically *oxidize* hydrogen under 1 atm of H_2 in CH_3CN solutions buffered with either $[^nBu_4N][CF_3CO_2]$ (for **1**) or $[^nBu_4N][TsO]$ (for **2**). No oxidation activity could be detected at scan rates between 100 and 1000 mV per second near the $Co^{II/I}$ potential. We attributed this to the slow reaction rates for H_2 oxidation catalyzed by **1** and **2**. In support of this view, H_2 *was oxidized* by **1** in the presence of $[^nBu_4N][CF_3CO_2]$ in CH_3CN over a period of several days, reaching an equilibrium mixture (Figure 8). The equilibrium constant for eq 8 is calculated to be ∼0.03 $atm^{1/2}$, corresponding to an overpotential of ∼90 mV for H_2 evolution by catalyst **1**. We did not observe similar H_2 oxidation by **2** in the presence of $[^nBu_4N][TsO]$ in CH_3CN over a few weeks, indicating that H_2 oxidation by **2** was appreciably slower.[36]

The overpotentials for H_2 evolution catalyzed by complexes **1** and **2** are among the smallest established for any synthetic complex. Considering the thermodynamic potentials of the acid used in each case,[28−30,35] the $Cp_2Mo_2S_2$ and $[Ni(P^{Ph}_2N^{Ph}_2)(CH_3CN)]^{2+}$ systems by DuBois et al. have estimated overpotentials of 120 mV and 570 mV, respectively, and the $[Co(dmgH)_2PyCl]$ system by Artero et al. has an overpotential of 180 mV. To the best of our knowledge, **1** is the first synthetic complex to be established to mediate both H_2 evolution and oxidation, enabling the direct measurement of its modest overpotential for H_2 evolution.

4. Conclusions

Cobalt complexes supported by macrocyclic glyoxime and tetraimine ligands catalyzed electrochemical H_2 evolution at potentials between −0.55 V and −0.20 V vs SCE in CH_3CN. The overpotentials for the electrocatalysis, relative to the thermodynamic potentials for H_2 evolution in acidic CH_3CN, are estimated to be small. Compared to literature values for the thermodynamic potential in CH_3CN, overpotentials are estimated to be ∼40 mV for **1** and ∼50 mV for **2**. Most significantly, we have shown experimentally that **1** can mediate both H_2 evolution and oxidation. We estimate from our equilibrium measurements of a solution containing both H_2 and acid that the overpotential is 90 mV for **1**.

The potential at which H_2 evolution occurs can be controlled by modulating the electronic properties of the ligand, with less electron donating ligands giving rise to a more easily reduced complex that catalyzes H_2 evolution at a more positive potential. However, for the series of Co complexes described here, the positive shift of the catalytic wave correlates with a decreased activity for electrocatalysis. Evidence for the existence of a Co(III)−H intermediate has been obtained from the cyclic voltammetric data. Digital simulations of the voltammetry of the electrocatalysis suggest that H_2 evolution catalyzed by **1** and **4a** in the presence of moderately weak acids in acetonitrile proceeds predominantly via a bimetallic mechanism. Ongoing work will attempt to more directly probe the mechanism of these H_2 evolving systems using stopped-flow methods.

5. Experimental Section

5.1. Chemicals and Reagents. All manipulations were carried out under an inert N_2(g) atmosphere using standard Schlenk or glovebox techniques. Unless otherwise noted, all solvents were deoxygenated by sparging with N_2(g) and were dried by passing through an activated alumina column. Prior to use, $HBF_4\cdot Et_2O$ and CF_3COOH were degassed by standard freeze−pump−thaw procedures. Deuterated solvents were purchased from Cambridge Isotope Laboratories, Inc., and were degassed and stored over activated 3 Å molecular sieves prior to use. All other reagents were purchased from commercial sources and used without further purification. *p*-Cyanoanilinium tetrafluorobate and anisidinium tetrafluoroborate were synthesized following the method reported by DuBois et al.,[9] with the exception that fluoroboric acid in ether was used as the acid source. Complexes **1**,[37] **2**,[13] **4a**,[17] **4b**,[19] **4c**,[19]**5a**,[20] **5b**,[19] **5c**[19], **6a**,[18] and **6b**[19] were synthesized according to literature methods; complex $Co(dmgBF_2)_2(CH_3CN)$ $CoCp_2$ was prepared as described before.[10]

5.2. Physical Methods. UV−vis measurements were carried out using a Varian Cary 50 Bio spectrophotometer controlled by Cary WinUV software. NMR spectra were recorded using a Varian Mercury 300 spectrometer. ^1H NMR chemical shifts were referenced to residual solvent as determined relative to Me_4Si ($\delta = 0$ ppm). $^{19}F\{^1H\}$ chemical shifts were referenced to an external standard (neat $BF_3\cdot Et_2O$, $\delta = 0$ ppm). X-ray diffraction studies were carried out in the Beckman Institute Crystallographic Facility on a Bruker Smart 1000 CCD Diffractometer.

Cyclic voltammetric measurements were recorded by a CHI 600B electrochemical analyzer that was connected to a glassy carbon working electrode (surface area = 0.07 cm^{-2}), a platinum wire auxiliary electrode, and a $Ag/AgNO_3$ (0.01 M) reference electrode filled with acetonitrile and $[^nBu_4][ClO_4]$ (0.1 M). All potentials were referenced to Fc/Fc^+ as an internal standard and were converted to SCE by adding 0.38 V to the measured potentials.[30] The concentrations of $HBF_4\cdot Et_2O$, $TsOH\cdot H_2O$, and CF_3COOH were calibrated by measuring the pH of aqueous solutions of known volume/quantity of the acids using a Beckman 32 pH meter.

Simulation of the cyclic voltammetry was performed using the DigiElch program by M. Rudolph.[32] The standard potentials for

(35) Daniele, S.; Ugo, P.; Mazzocchin, G. A.; Bontempelli, G. *Anal. Chim. Acta* **1985**, *173*, 141−148. Wayner, D. D. M.; Parker, V. D. *Acc. Chem. Res.* **1993**, *26*, 287−294. Ellis, W. W.; Raebiger, J. W.; Curtis, C. J.; Bruno, J. W.; DuBois, D. L. *J. Am. Chem. Soc.* **2004**, *126*, 2738−2743.

(36) One reviewer suggested that the pK_a for $TsOH(H_2O)$ should be about 7 in acetonitrile due to a large self-association constant upon deprotonation. If this is true, the overpotential for **2** will be 109 mV, probably too large for H_2 oxidation by **2** to be observed.

(37) Bakac, A.; Espenson, J. H. *J. Am. Chem. Soc.* **1984**, *106*, 5197−5202.

electron-transfer reactions (1) and (3) were taken from cyclic voltammetric measurements. The rate of charge transfer was set as 10^5 cm/s ($\alpha = 0.5$). A diffusion coefficient of 10^{-5} cm^2 s^{-1} was assumed for all acid present in the reaction mixture, and a semi-infinite 1-D diffusion model was used in the simulation. The geometry of the electrode was assumed to be planar. See Supporting Information for detailed parameters.

Bulk electrolysis experiments were done in a custom-made, gastight, H-type cell that was equipped with a reticulated vitreous carbon working electrode (BAS), a $Ag/AgNO_3$ reference electrode, and a coiled Pt counter electrode. The counter electrode was separated from the working electrode by a glass frit. The amount of H_2 gas evolved was quantified by analyzing the gas mixture in the headspace using a Thermo Finnigan DeltaplusXP system equipped with Finnigan trace GC and an Isotope Ratio Mass spectrometer. The total amount of H_2 produced was calculated as the sum of the H_2 in the headspace plus H_2 dissolved in the solvent (calculated using Henry's Law, with a constant of 275 atm^{-1}).

5.3. Synthesis of [Co(dpgBF$_2$)$_2$]CoCp$_2$ (3·CoCp$_2$). A solution of $CoCp_2$ (32 mg, 0.17 mmol) in CH_3CN was added to a solution of **2** (113 mg, 0.17 mmol) in CH_3CN at room temperature. The reaction mixture was stirred for 2 h before being evaporated to dryness. The resulting purple solid was collected on a filter frit, washed with diethyl ether, and dried in a vacuum. Yield: 110 mg (75%). ^{1}H NMR (300 MHz, CD_3CN): $\delta = 7.35$ (bs, 20 H), 5.63 (s, 10 H) ppm. ^{19}F{^{1}H} NMR (282 MHz, CD_3CN) : $\delta = 153.2$ (m, 4F). Anal. Calcd for $C_{40}H_{33}F_4N_5B_2O_4Co_2$: C, 55.66%; H, 3.85%; N, 8.11%. Found: C, 55.33%; H, 3.93%; N, 8.09%. [Co(dpgBF$_2$)$_2$]CoCp$_2$ (**3·Na**) can be synthesized similarly, using Na/Hg instead of $CoCp_2$ as the reductant.

5.4. Crystallographic Details for [Co(dpgBF$_2$)$_2$(CH$_3$CN)$_2$]·2CH$_2$Cl$_2$ (2). Single crystals suitable for X-ray diffraction studies were grown by diffusion of diethyl ether into a solution of **2** in CH_2Cl_2 that had been spiked with a few drops of CH_3CN. A crystal of dimensions 0.20 mm × 0.10 mm × 0.05 mm^3 was obtained and was mounted onto a glass fiber. A total of 18 190 reflections ($-10 \le h \le 12$, $-34 < k \le 32$, $-19 \le l \le 19$) were collected at $T = 100(2)$ K in the range of 1.58° to 28.23° of which 4305 were unique ($R_{int} = 0.1177$); Mo Kα radiation ($\lambda = 0.710\,73$ Å). The structure was solved by the Direct method. All non-hydrogen atoms were refined anisotropically, and hydrogen atoms were placed in calculated idealized positions. The residual peak and hole electron densities were 1.643 and -1.356 eA^{-3}, respectively. The absorption coefficient was 0.793 mm^{-1}. The least-squares refinement converged normally with residuals of $R(F) = 0.0619$, $wR(F^2) = 0.0901$, and a GOF = 1.316 ($I > 2\sigma(I)$). $C_{34}H_{30}B_2Cl_4CoF_4N_6O_4$, space group $C2/c$, monoclinic, $a = 9.8460(4)$ Å, $b = 25.7081(13)$ Å, $c = 15.1519(6)$ Å, $\alpha = 90.00$ °, $\beta = 91.535(2)$°, $\gamma = 90.00$ °, $V = 3833.9(3)$ Å^3, $Z = 4$, $\rho_{calcd} = 1.533$ Mg/m^3.

5.5. Crystallographic Details for [Co(dpgBF$_2$)$_2$(CH$_3$CN)](Na(12-C-4)$_2$)·CH$_3$CNEt$_2$O (3·Na(12-C-4)$_2$). Single crystals suitable for X-ray diffraction study were grown by diffusion of diethyl ether into a solution of **3·Na** in CH_3CN in the presence of 2 equiv of 12-crown-4. A crystal of dimensions 0.15 mm × 0.08 mm × 0.05 mm was obtained and was mounted onto a glass fiber. A total of 79 724 reflections ($-16 \le h \le 16$, $-19 \le k \le 19$, $-39 \le l \le 38$) were collected at $T = 100(2)$ K in the range of 1.37° to 28.55° of which 12 962 were unique ($R_{int} = 0.0830$); Mo Kα radiation ($\lambda = 0.710\,73$ Å). The structure was solved by the Direct method. All non-hydrogen atoms were refined anisotropically, and hydrogen atoms were placed in calculated idealized positions. One acetonitrile solvent molecule and one diethyl ether solvent molecule were found in each asymmetric unit. These solvent molecules were severely disordered and could not be refined accurately. The residual peak and hole electron densities were 1.374 and -0.980 eA^{-3}, respectively. The absorption coefficient was 0.402 mm^{-1}. The least-squares refinement converged normally with residuals of $R(F) = 0.0554$, $wR(F^2) = 0.1016$ and a GOF = 1.042 ($I > 2\sigma(I)$). $C_{202.18}H_{236.64}N_{23.01}O_{51.04}F_{16}Na_4Co_4B_8$, space group $P2(1)/n$, monoclinic, $a = 12.444(2)$, $b = 14.709(3)$, $c = 29.884(6)$, $\alpha = 90°$, $\beta = 93.319(5)°$, $\gamma = 90°$, $V = 5461.0(19)$ Å^3, $Z = 5$, $\rho_{calcd} = 1.376$ Mg/m^3.

Acknowledgment. We acknowledge support from an NSF Chemical Bonding Center (grant CHE-0533150) and from the Beckman Institute Molecular Materials Research Center. We thank Prof. Nathan S. Lewis, Prof. Harry B. Gray, and Dr. Jay Winkler for insightful discussions. We also thank Prof. Alex Sessions and Dr. Chao Li for their generous help with the gas chromatography measurements and Neal Mankad and Larry Henling for help with crystallographic studies.

Supporting Information Available: Steady state analysis for the rate law of electrocatalysis; electrocatalysis of **4a** in HBF_4·Et_2O, of **4b** in TsOH·H_2O and HBF_4·Et_2O, and of **5a**−**b** in HBF_4·Et_2O; variations of catalytic currents i_c on the concentrations of catalyst and acid for **2**, **4a**, and **4b**; simulation of catalytic waves for **1**, **2**, **4a**, and **4b**; catalytic waves of **2** and **4a** showing evidence of cobalt(III) hydrides; and crystallographic data for **2** and **3**. This information is available free of charge via the Internet at http://pubs.acs.org.

JA067876B